Finite volume effects on QCD susceptibilities with a chiral chemical potential

Run-Lin Liu,[1,*] Meng-Yun Lai,[2,†] Chao Shi,[3,‡] and Hong-Shi Zong[1,4,5,§]

[1]*Department of Physics, Nanjing University, Nanjing 210093, China*
[2]*College of Physics and Communication Electronics Jiangxi Normal University, Nanchang, Jiangxi 330022, China*
[3]*Department of Nuclear Science and Technology, Nanjing University of Aeronautics and Astronautics, Nanjing 210016, China*
[4]*Joint Center for Particle, Nuclear Physics and Cosmology, Nanjing 210093, China*
[5]*Department of Physics, Anhui normal University, Anhui 241102, China*

(Received 28 February 2020; accepted 12 June 2020; published 10 July 2020)

The finite volume effect on the QCD phase diagram is investigated via the two-flavor Polyakov-loop-modified Nambu-Jona-Lasinio model in the presence of the chiral chemical potential within the mean-field approximation. Our calculations concentrate on the quark condensate, chiral number density and its derivative, namely, QCD susceptibilities. We find the chiral number density decreases as the system size gets smaller. It is also confirmed that the volume of the strongly interacting matter has an influence on the phase diagram, in particular on the crossover region and the location of a chiral transition line. Therefore, the critical end point (CEP) also shifts with system size. On this basis it follows that study of the finite volume effect as well as the chiral chemical potential dedicated to the chiral phase transition and probing the location of the CEP.

DOI: 10.1103/PhysRevD.102.014014

I. INTRODUCTION

As an essential part of the Standard Model of particle physics, quantum chromodynamics (QCD) is the fundamental theory of strong interaction between quarks and gluons in the Universe. Discussions regarding the phase diagram of QCD matters have dominated research over decades. Moreover, the search for the critical end point (CEP) on the phase diagram has been propelled to the forefront in recent years from both theories [1–16] [such as lattice QCD, Dyson-Shwinger Equations (DSEs), Nambu-Jona-Lasinio model (NJL) and related Polyakov-loop-extended Nambu-Jona-Lasinio (PNJL) model, etc.] and experiments [17–20] [e.g., the BNL Relativistic Heavy-Ion Collider (RHIC) and the CERN Large Hadron Collider (LHC)]. Unfortunately, vigorous evidence of the existence of the CEP is still absent from the first principles of QCD since present lattice QCD calculations at finite chemical potential are plagued with the so-called "sign problem" [21,22].

The QCD phase diagram is further complicated with the presence of a chiral chemical potential μ_5, which conjugates to the chiral charge density. The nonvanishing μ_5 mimics the chirality imbalance generated in event-by-event quark-gluon plasma production. It also has been introduced to probe the existence and location of the CEP by Refs. [23–29]. In particular, continuation of the critical line from the area of chiral chemical potential to that of quark chemical potential comes into realization, which predicts that the CEP in the $T-\mu$ plane ($\mu_5 = 0$ MeV) can be obtained by continuation of the critical end point (CEP_5) in the $T-\mu_5$ plane ($\mu = 0$ MeV) [24–26]. Nevertheless, lattice QCD simulation [28,30] and DSEs [31,32] demonstrates that there is no CEP_5 in the $T-\mu_5$ plane. On the other hand, the chirality imbalance induces the generation of electric current along an external magnetic field, which is named the chiral magnetic effect (CME). Hence, it is important to consider the effect of the chiral chemical potential, and it will contribute much to a further insight of the chiral phase transition.

The QGP fire ball formed in relativistic heavy-ion collisions apparently has a finite volume whose radii are estimated to be 2 to 10 fm, depending on the center of mass energy, the size of the colliding nuclei, and the centrality of collisions, etc. [33–36]. Therefore, in order to better understand the results of relativistic heavy ion collision experiments, we need to study the effect of finite volume effects on the strong interaction phase diagram. A recent review of the finite volume effect [37] purports that the study of the finite volume effect not only attracted great academic interest but also served as a check on the algorithm and simulation method. And the survey of the finite volume effect [38–40] has become more and more

*phyrunlin@smail.nju.edu.cn
†mengyunlai@jxnu.edu.cn
‡cshi@nuaa.edu.cn
§zonghs@nju.edu.cn

relevant with the steady promotion of lattice QCD, which carries out the numerical calculations with finite lattices in finite and discrete Euclidean space-time, and finite size scaling analysis can be regarded as a worthy implement to research the chiral phase transition in QCD [41–45]. Widely accepted, finite volume effects have significantly influenced investigation of different kinds of physical systems such as ultracold atoms in optical lattices over condensed matter systems [46–50], multilayer systems, and relativistic heavy-ion collisions [51–57].

As mentioned above, research of the effect of the chiral chemical potential on the chiral phase transition have been carried out by Refs. [31,32,52,58,59], while Refs. [60–69] have taken the finite volume effects into consideration to probe the deviation of QCD phase diagram. On this basis, to better understand the results of relativistic heavy ion collision we take account of the chiral chemical potential and the finite volume effects simultaneously to provide deep insight into the chiral phase transition. In this paper we study the susceptibilities χ_s (chiral susceptibility) and χ_T (temperature susceptibility) in the presence of the finite volume effect and the chiral chemical potential, and depict the phase diagram in this analysis. As a measure of fluctuation effects of the physical system, which means the linear response to external fields, susceptibilities play significant roles in the depiction of phase transition phenomenon. Hence, considering the chiral chemical potential and the finite volume effect simultaneously to investigate the susceptibilities may lead to a better understanding of the chiral phase transition. We will also investigate the finite volume effects on the chiral charge density n_5, which is relevant for CME. As far as we know, this is a first investigation for such effect.

The rest of this paper is organized as follows: In Sec. II, we give a basic description of the two-flavor PNJL model with chiral chemical potential. In Sec. III we introduce the PNJL Lagrangian density in a finite volume and demonstrate the results. In Sec. IV, we give a summary and conclusion.

II. PNJL MODEL WITH CHIRAL CHEMICAL POTENTIAL AND PHASE DIAGRAM

The Lagrangian density of the two flavor PNJL model for equal-mass quark can be written as follows:

$$\mathcal{L} = \bar{\psi}(\gamma \cdot \not{D} + m)\psi + G[(\bar{\psi}\psi)^2 + (\bar{\psi} i\gamma_5 \boldsymbol{\tau}\psi)^2] + \mathcal{U}(\Phi, \bar{\Phi}, T), \tag{1}$$

where $\psi = (u, d)$ represents the quark field in the fundamental representation of the flavor $SU(2)$, and we take the number of colors $N_c = 3$, m is the current quark mass, G is the coupling constant of four-fermion interaction, $\boldsymbol{\tau}$ corresponds to the Pauli matrices in flavor space, and $\mathcal{U}(\Phi, \bar{\Phi}, T)$ is a Polyakov-loop effective potential throughout this work.

The Polyakov loop is a Wilson loop which is designed to solve the QCD confinement problem in compactified Euclidean space-time, and can be given by

$$L(x) = \mathcal{P}\exp\left[-i\int_0^\beta dx_4 A_4(x_4, \vec{x})\right], \tag{2}$$

where $\mathcal{P}$ denotes the path ordering; $\beta = 1/T$, namely, the reciprocal of temperature. Besides, the Polyakov gauge in which L is diagonal in color space [70] is applied here. And for simplicity we take the approximation $L^\dagger = L$ following Refs. [25,26]. Then the mean-field effective potential of the PNJL model can be written in terms of

$$\Phi = \frac{1}{N_c}\mathrm{Tr}_c L, \tag{3}$$

$$\bar{\Phi} = \frac{1}{N_c}\mathrm{Tr}_c L^\dagger. \tag{4}$$

Then $\Phi = \bar{\Phi}$ can be easily obtained without any doubt. The form of the Polyakov-loop effective potential is provided to reproduce the gluonic lattice data in the classical background by Ref. [13]:

$$\begin{aligned}\beta^4\mathcal{U}(\bar{\Phi}, \Phi; T) &= \beta^4\mathcal{U}(\Phi; T) \\ &= \left[-\frac{1}{2}a(T)\Phi^2 + b(T)\ln(1 - 6\Phi^2 + 8\Phi^3 - 3\Phi^4)\right],\end{aligned} \tag{5}$$

in which the model parameters are temperature dependent,

$$a(T) = a_0 + a_1\left(\frac{T_0}{T}\right) + a_2\left(\frac{T_0}{T}\right)^2, \quad b(T) = b_3\left(\frac{T_0}{T}\right)^3, \tag{6}$$

with the parameters set as Refs. [4,71],

$$a_0 = 3.51, \quad a_1 = -2.47, \quad a_2 = 15.2, \quad b_3 = -1.75. \tag{7}$$

In the PNJL model, the confinement-deconfinement phase transition is described by Polyakov loop.

The chiral chemical potential μ_5, conjugated to the chiral charge density, $n_5 = n_R - n_L$, is introduced to emulate imbalance between right- and left-handed quarks. As a result, to investigate the effects of μ_5 we add the following term to the PNJL Lagrangian:

$$-\mu_5\bar{\psi}\gamma_0\gamma_5\psi, \tag{8}$$

which induces the chiral number density

$$n_5 = \langle\bar{\psi}\gamma_0\gamma_5\psi\rangle. \tag{9}$$

Adopting the mean-field approximation, the thermodynamic effective potential obtained at the one-loop level is given by Ref. [25],

$$\begin{aligned}\Omega &= \Omega(M,\Phi;T,\mu,\mu_5)\\ &= \mathcal{U}(\Phi;T) + \frac{(M-m)^2}{4G} - 2N_c\sum_{s=\pm1}\int\frac{d^3\vec{p}}{(2\pi)^3}\omega_s\\ &\quad -\frac{2}{\beta}\sum_{s=\pm1}\int\frac{d^3\vec{p}}{(2\pi)^3}\ln[\mathcal{F}_+\mathcal{F}_-],\end{aligned} \tag{10}$$

where M is the effective quark mass and relates to the quark condensate $\langle\bar{\psi}\psi\rangle$ as

$$M = m - 2G\langle\bar{\psi}\psi\rangle, \tag{11}$$

and the quasiparticle dispersion ω_s is

$$\omega_s = \sqrt{(s|\vec{p}| - \mu_5)^2 + M^2}, \tag{12}$$

in which s means the helicity projection. In addition, the functions $\mathcal{F}_\pm$ in Eq. (10), which contribute to the statistical thermal properties, quark confinement, in the low temperature region is written as

$$\mathcal{F}_\pm = 1 + 3\Phi[e^{-\beta\omega_s^\pm} + e^{-2\beta\omega_s^\pm}] + e^{-3\beta\omega_s^\pm}, \tag{13}$$

where the $\omega_s^\pm = \omega_s \pm \mu$. The chiral number density can be gotten as the derivative of Ω,

$$n_5 = -\frac{\partial\Omega}{\partial\mu_5}. \tag{14}$$

The other parameters used in this paper are given by Ref. [72]: $T_0 = 190$ MeV; $m = 5.5$ MeV, $\Lambda = 631$ MeV, $G = 5.074\times10^{-6}$ MeV^{-2}, which are determined by fitting the pion mass $m_\pi = 138$ MeV; the pion decay constant $f_\pi = 93.1$ MeV. Through

$$\frac{\partial\Omega}{\partial M} = 0, \qquad \frac{\partial\Omega}{\partial\Phi} = 0 \tag{15}$$

we can get the effective quark mass and the mean-field effective potential for any given T, μ, and μ_5. Afterwards, the quark condensate can be determined through Eq. (15). Then two kinds of QCD susceptibilities, the first derivative of the quark condensate, applied to study of the chiral phase transition in the analysis are defined as

$$\chi_s = -\frac{\partial\langle\bar{\psi}\psi\rangle}{\partial m}, \tag{16}$$

$$\chi_T = \frac{\partial\langle\bar{\psi}\psi\rangle}{\partial T}. \tag{17}$$

In the processing, the divergence of the momentum integral for ω_s must be cured by a regularization procedure. Therefore, a momentum cutoff, viz., Λ, is employed for the following two terms.

$$\begin{aligned}\Omega_V &= 2N_c\sum_{s=\pm1}\int\frac{d^3\vec{p}}{(2\pi)^3}\omega_s,\\ \Omega_{\mathcal{F}} &= \frac{2}{\beta}\sum_{s=\pm1}\int\frac{d^3\vec{p}}{(2\pi)^3}\ln[\mathcal{F}_+\mathcal{F}_-].\end{aligned} \tag{18}$$

Reference [59] has given a detailed argument about the spirit of this choice: the contact interaction can broadly be reconciled with QCD while the necessary regularization function is a useful representation of the transition between nonperturbative infrared dynamics, such as gluon mass generation [73–76], and the domain of asymptotic freedom, which indicates that internal consistency requires one to employ the same cutoff.

Regardless of the chiral limit or nonchiral limit, we need to point out that in many cases Eq. (15) has three solutions. One of the solutions yields a global minimum of the effective potential corresponding to the physical state, the second gives the local minimum which indicates the metastable state, and the last one giving a maximum predicts an unstable state. Just as the declaration in Refs. [77,78], the last solution is only a mathematical solution with no physical meaning. Therefore, we will only study the physical and metastable solutions mentioned above. At low temperature or low chemical potential, the physical solution is often referred to as the Nambu solution, where the chiral symmetry is dynamically broken. The metastable solution is named the pseudo-Winger solution by Ref. [78], which reflects that the chiral symmetry is partially restored as shown in Refs. [77,78]. In the chiral limit, the pseudo-Winger solution obtained beyond the chiral limit will degenerate to the well-known Winger solution. The so-called strong interaction chiral phase transition is essential to study the evolution of the Nambu and pseudo-Winger solutions with temperature and chemical potential, and in particular to study the competitive relationship between the two solutions at different temperature and chemical potential. We calculate the effective quark mass and the susceptibilities for certain μ, μ_5, and T. As shown in Fig. 1, the effective quark mass is discontinuous at $T = 80$ MeV and the first-order phase

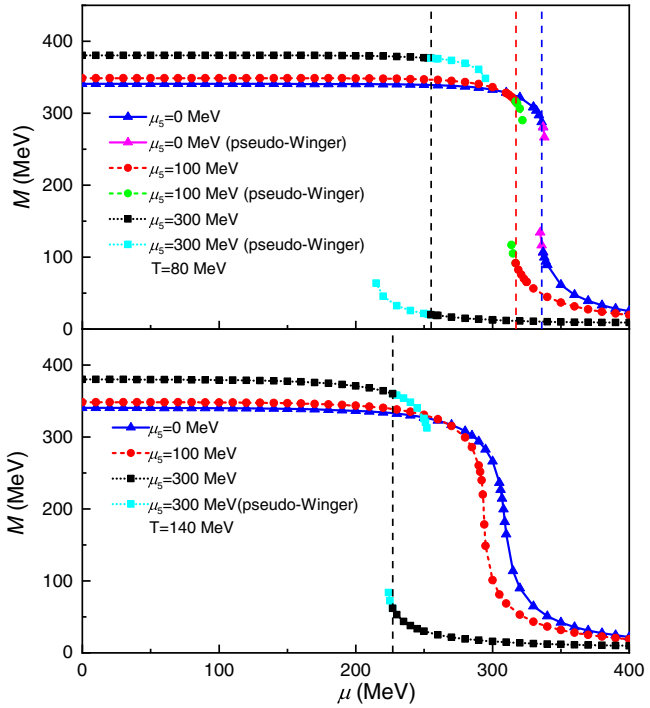

FIG. 1. The effective quark mass as a function of μ for different T and μ_5.

transition points for $\mu_5 = 0$, 100, 300 MeV are located at $\mu = 336, 317, 255$ MeV, respectively, which suggests the decrease of μ associated with the first-order phase transition as μ_5 increase. Besides, the effective quark mass turns to a crossover for $\mu_5 = 0$ and 100 MeV while M is yet discrete for $\mu_5 = 300$ MeV at $T = 140$ MeV. And the first-order phase point at $\mu_5 = 300$ MeV is $\mu = 227$ MeV. Thereby the results contend that the temperature of the CEP increase with μ_5, which is consistent with lattice QCD [13,23,28] and DSEs [32].

Moreover, the chiral susceptibility χ_s and temperature susceptibility χ_T, which are studied as functions of chemical potential μ for different chiral chemical potential μ_5, are depicted in Fig. 2. We used two values of the temperature T to exhibit the characteristics of susceptibilities in the first-order phase transition region and the crossover region, respectively. The upper panel of Fig. 2 demonstrates two features. First, the value of μ for the first-order phase transition decreases with increasing μ_5, which has already been observed from Fig. 1. Another one is that two different susceptibilities have the same break point at $T = 80$ MeV for three different values of μ_5, which results from the fact that both χ_s and χ_T are the first derivative of the quark condensate. At high temperature $T = 160$ MeV, the two susceptibilities at $T = 160$ MeV shift to a continuous crossover instead of a chiral phase transition, as indicated in the lower panel of Fig. 2, although the μ of the peak point of χ_s differ from χ_T.

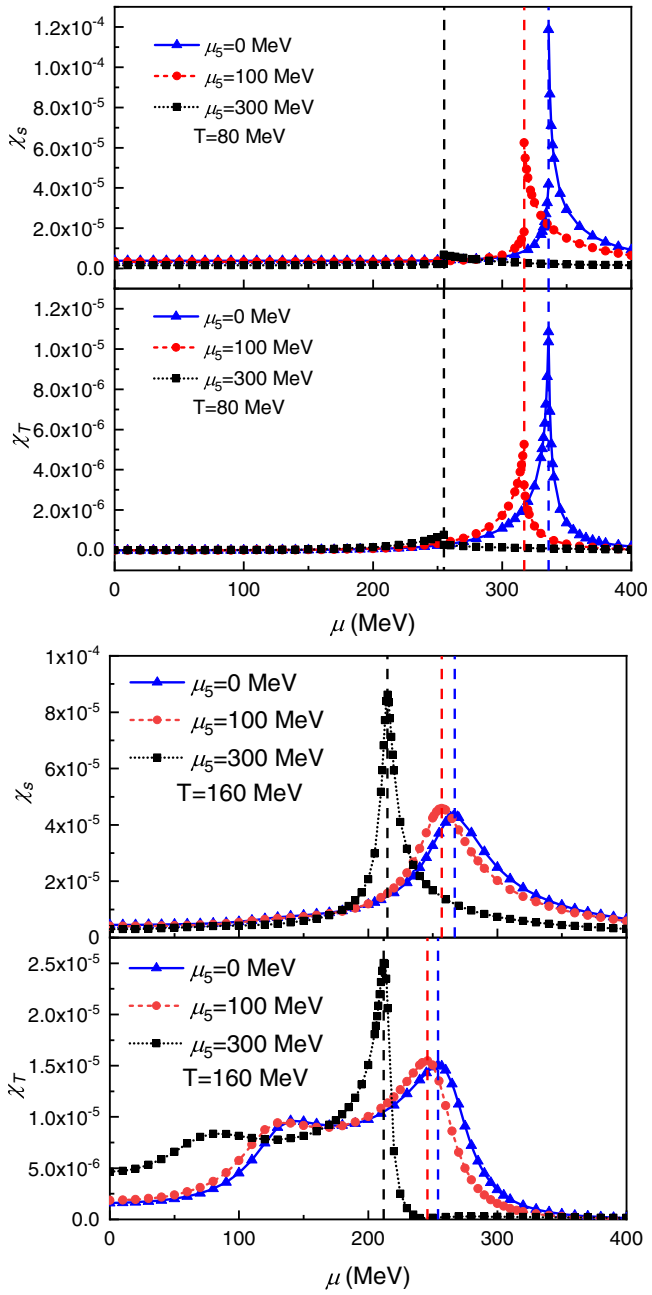

FIG. 2. The chiral susceptibility χ_s and the temperature susceptibility χ_T as a function of μ for different T and μ_5.

III. THE FINITE VOLUME EFFECTS ON THE CHIRAL PHASE TRANSITION

As mentioned above, the properties of the hot dense matter formed in the heavy-ion collisions relate to its finite volume, which probably sheds light on a distinct QCD phase structure. Furthermore, the detection of the curious finite volume effects in QCD vacuum can give us a clear comprehension of the dynamical chiral symmetry breaking as well as the partial restoration of chiral symmetry [41,79–83].

In recent decades, a variety of diverse techniques, i.e., renormalization group methods [84–86], chiral perturbation theory [82,87,88], and random matrix theory [81,89,90], have served as analytical tools to study the finite volume constraints. To implement the finite volume constraints, we choose specific boundary conditions: periodic for bosons and antiperiodic for fermions, which lead to a infinite sum over discrete momentum values $p_i = \pi n_i/R$, where $i = x, y, z$, and n_i represents integers (odd for fermion and even for boson) and R is the lateral size of a cubic volume. Such choice can be approximated by implementing a lower momentum cutoff $p_{\min} = \lambda = \frac{\pi}{R}$ following Refs. [51,60,91]. Thereby, the expression of the thermodynamic effective potential incorporating the finite volume effect is

$$\Omega = \mathcal{U}(\Phi; T) + \frac{(M-m)^2}{4G} - 2N_c \sum_{s=\pm 1} \int_{\lambda}^{\Lambda} \frac{d^3\vec{p}}{(2\pi)^3} \omega_s - \frac{2}{\beta} \sum_{s=\pm 1} \int_{\lambda}^{\Lambda} \frac{d^3\vec{p}}{(2\pi)^3} \ln\left[\mathcal{F}_+ \mathcal{F}_-\right]. \tag{19}$$

Then it follows that Eq. (19) reduces to the infinite volume case while $\lambda = 0$, namely, $R = \infty$. To carry out the analysis, we have taken into consideration various system sizes, viz. $R = 3$, $R = 5$, and $R = 10$ fm, to calculate the effective quark mass, chiral number density, and susceptibilities as in the previous section.

As shown in Fig. 3, M as a function of μ is discontinuous for $R = \infty$, 10, 5 fm while the discontinuity of M vanishes for $R = 3$ fm in the upper panel at $T = 80$ MeV and $\mu_5 = 0$, 100 MeV. Furthermore, we can find that the $R = \infty$ curve almost coincides with that of $R = 10$ fm at the range of $\mu \in [0, 400]$ MeV, and so does to the first-order phase transition point. While the system size is $R = 5$ fm, the Nambu solutions of M reduce slightly, meanwhile the pseudo-Winger solutions of M remain the same. However, the Nambu solutions of M have a prominent reduction and yet the pseudo-Winger solutions still have no obvious change as R decrease to 3 fm. In the meantime, the first-order phase transition turns to a crossover. The lower panel of Fig. 3 depicts the finite volume effects on the crossover regime at $T = 140$ MeV, which demonstrates almost the same effect on M as in the first-order phase transition region at $T = 80$ MeV. As a result, it is found that the effect of finite size on the Nambu phase is greater than that of the pseudo-Winger phase. In the PNJL model, people often adopt dynamic quark mass M to describe the chiral symmetry of the thermodynamics system, and use the Polyakov loop Φ to reflect the confinement behavior of the system. It should be noted that there is no rigorous order parameter for the deconfinement transition in the presence of dynamical quarks, but the Polyakov loop still can serve as a good indicator of a rapid crossover towards deconfinement. Next we study the effect of the finite size on Φ.

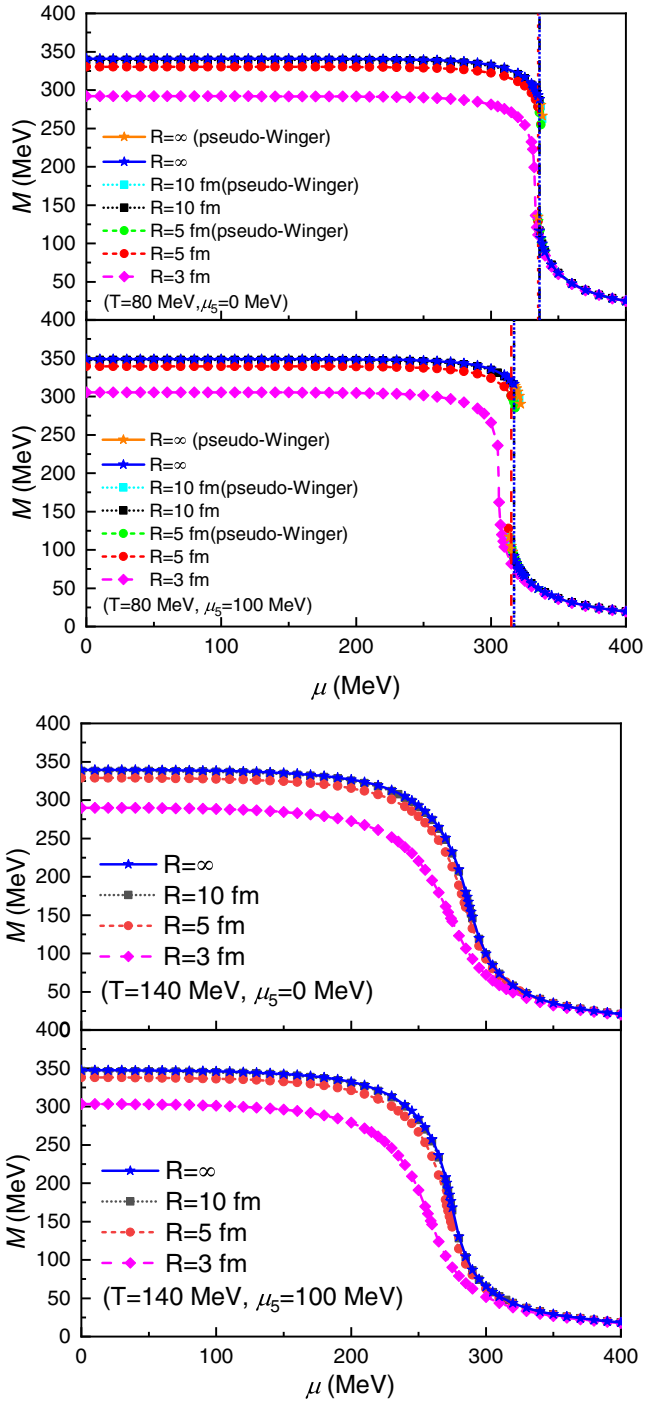

FIG. 3. Effective quark mass M with different R at $T = 80$, 140 MeV, and $\mu_5 = 0$, 100 MeV. The first-order phase transition points for $R = \infty$, 10, 5 fm are at $\mu = 336, 336, 335$ MeV at $T = 80$ MeV with zero μ_5 while the counterpart points at $\mu_5 = 100$ MeV are $\mu = 317$, 317, 315 MeV, respectively.

In the pure-gauge theory $\Phi = 0$ defines the confinement phase, whereas the deconfinement phase is expressed via $\Phi \neq 0$ and $\Phi = 1$ defines the entire deconfinement phase.

In Fig. 4, we depict variation of the Polyakov loop $\Phi(\mu)$ with decreasing system size for different T and μ_5. In the upper panel of Fig. 4 ($T = 80$ MeV), it can be found that $\Phi(\mu)$ is discontinuous at $R = \infty, 10, 5$ fm while the discontinuity of Φ vanishes at $R = 3$ fm for both $\mu_5 = 0$, 100 MeV. At $\mu_5 = 0$ MeV the corresponding first-order phase transition (deconfinement transition) points for $R = \infty, 10, 5$ fm are at $\mu = 336, 336, 335$ MeV, respectively,

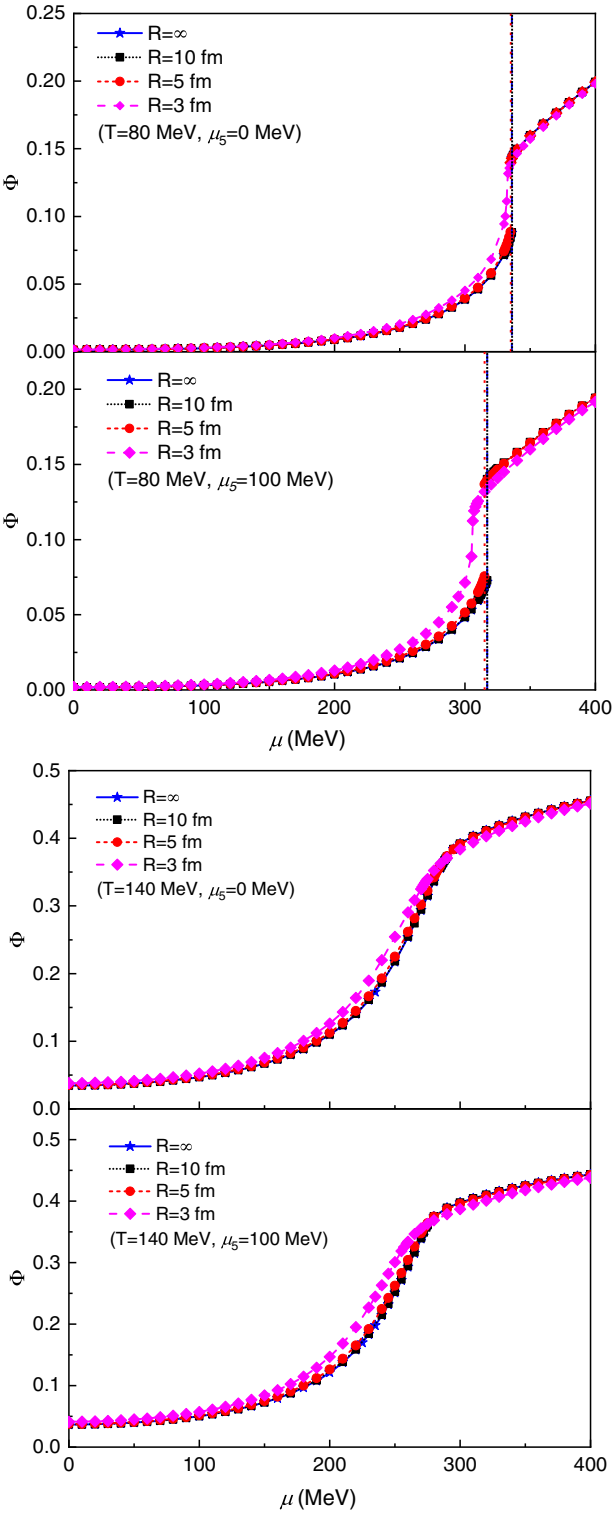

FIG. 4. The Polyakov loop Φ. The first-order phase transition points for $R = \infty$, 10, 5 fm are at $\mu = 336, 336, 335$ MeV at $T = 80$ MeV with zero μ_5 while the counterpart points at $\mu_5 = 100$ MeV are $\mu = 317, 317, 315$ MeV, respectively.

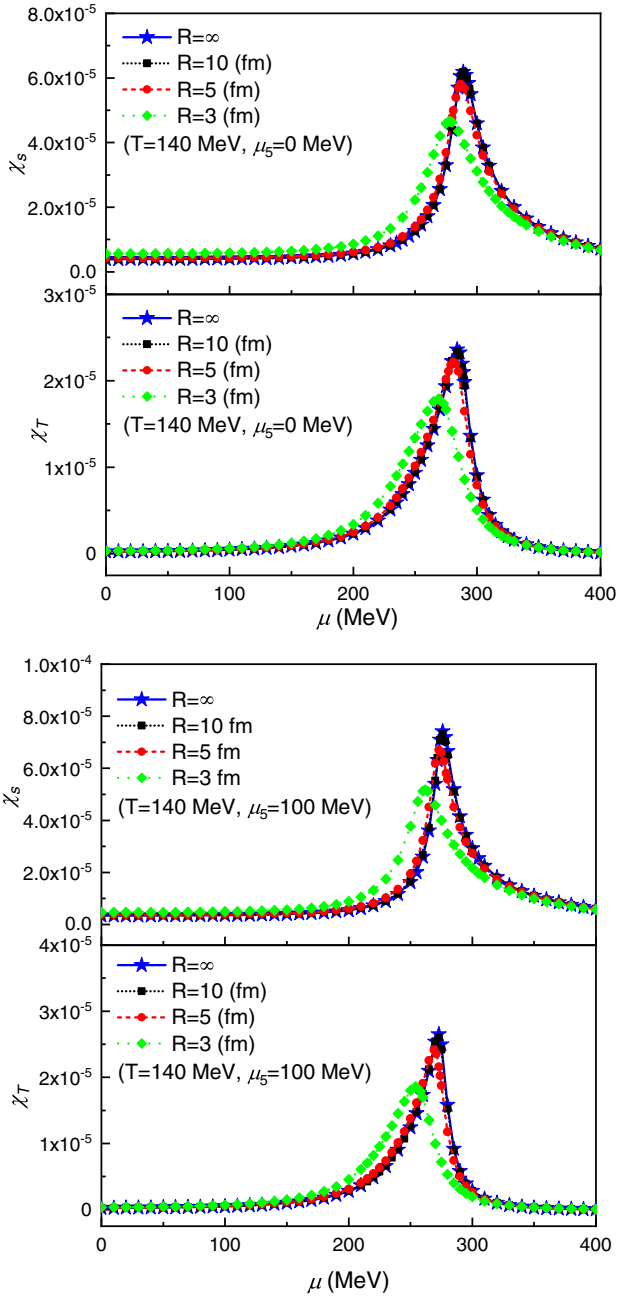

FIG. 5. χ_s and χ_T different R at $T = 140$ MeV and $\mu_5 = 0$, 100 MeV. The location of the peak points of χ_s for $R = \infty, 10, 5, 3$ fm without μ_5 is at $\mu = 289, 289, 287, 278$ MeV, respectively. And the corresponding points at $\mu_5 = 100$ MeV are $\mu = 276, 276, 273, 262$ MeV. And for χ_T the corresponding points at $\mu_5 = 0$ MeV are $\mu = 284, 284, 281, 269$ MeV while the corresponding points are $\mu = 273, 272, 269, 254$ MeV at $\mu_5 = 100$ MeV.

while at $\mu_5 = 100$ MeV, the corresponding first-order phase transition points are at $\mu = 317, 317, 315$ MeV. We also find that the finite system size has greater influence on the Φ around the phase transition point than in the low density where $\Phi(\mu)$ almost remain unchanged. The smaller R is, the greater effects it has on Φ. The lower panel of Fig. 4 at $T = 140$ MeV exhibits that all $\Phi(\mu)$ are continuous, which indicates the crossover transition. In addition, the finite size has greater effects on Φ around the crossover than in other regions where Φ almost stays the same as in the upper panel. Based on these, we hold that the finite volume constraint, implemented by the boundary condition we choose, has significant effects on the confinement behavior in the vicinity of the transition area. In some cases, it could even convert the first-order deconfinement transition into crossover.

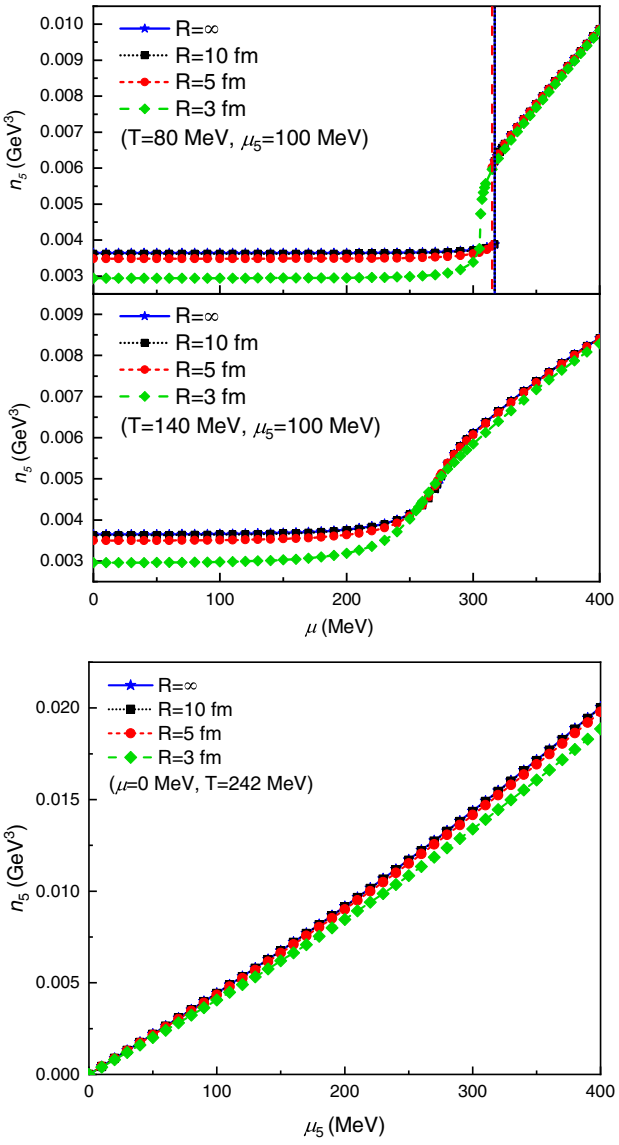

FIG. 6. The chiral number density.

We exhibits the variation of χ_s and χ_T with different R at the crossover region ($T = 140$ MeV). The curve of $R = 10$ fm is still the same as that of $R = \infty$, as shown in Fig. 5. The height of the peak of χ_s and χ_T is gradually suppressed while the system size R decreases from 10 to 3 fm for $\mu_5 = 0$, 100 MeV, and the μ of the peak decreases obviously at the same time. This is in agreement with the general understanding that the finite volume effect smears the transition area. Besides, the μ of the peak of χ_s differs from that of χ_T, which would lead to a crossover band in the $T - \mu$ phase diagram which has been argued by Refs. [92,93].

The chirality imbalance has an impact on the chiral magnetic effect, thus it is necessary to study the finite volume effect on the chiral number density n_5, which has been demonstrated in Fig. 6. It can be observed that n_5 is indeed depressed prominently with the decreasing R in the low μ region while the system size hardly affects n_5 in the high μ region from the upper panel of Fig. 6. The lower panel of Fig. 6 exhibits variation of the curve for n_5 which is set as a function of μ_5 with the reduction of R at $T = T_c = 242$ MeV. We observe that as the size of the system gets smaller, the n_5 also gets decreased. This suggests that in the study of CME, the finite volume effects

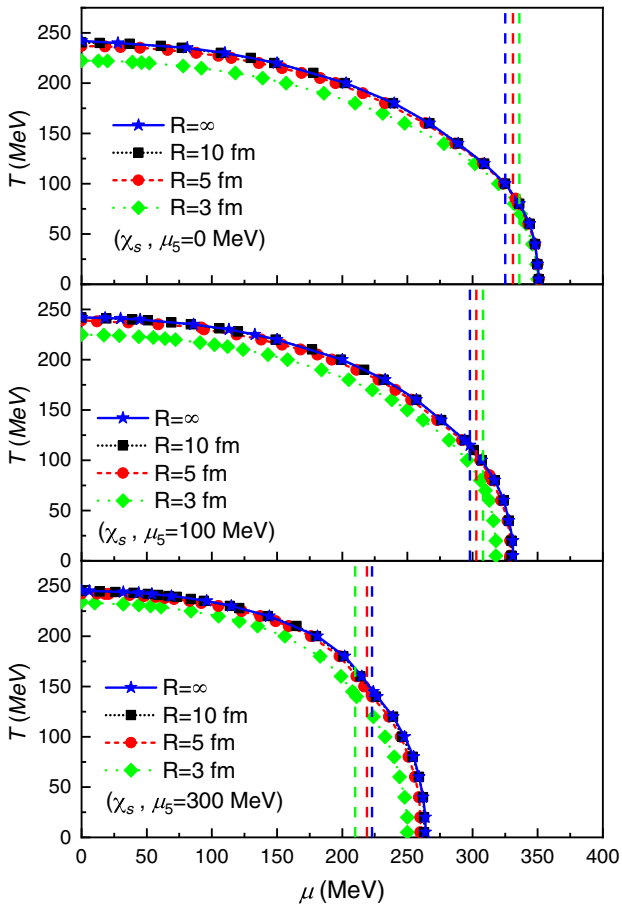

FIG. 7. The phase diagram determined by χ_s.

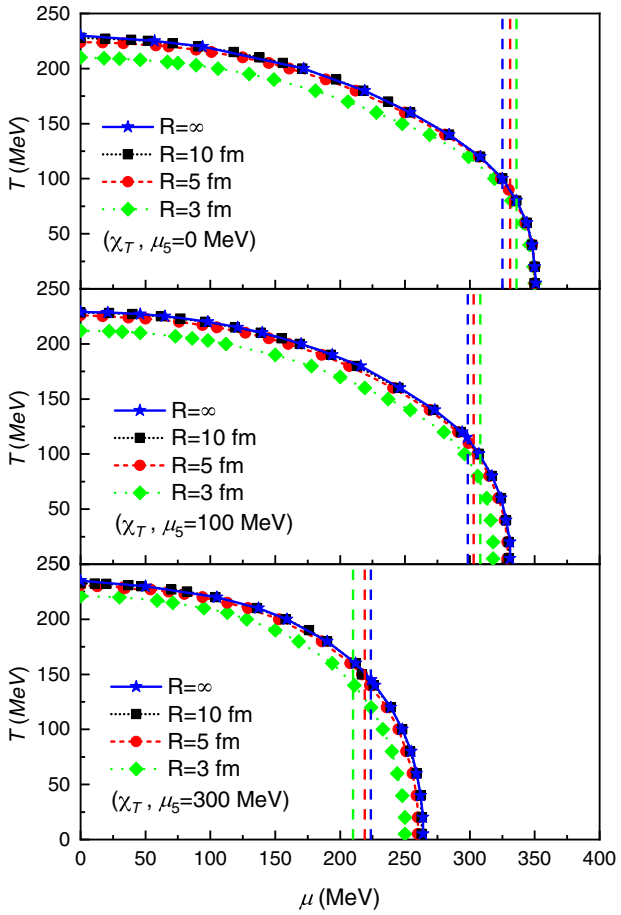

FIG. 8. The phase diagram determined by χ_T.

may suppress the chiral charge density, thereby affecting the induced electric current.

We turn now to the discussion of the phase diagram in the $T-\mu$ plane with different system size in Figs. 7 and 8, where the right side of the vertical dashed lines represents the first-order phase transition lines and the left side stands for the crossover region. It can be observed from the two figures that at $\mu_5 = 0$ MeV the system size almost has no effect on the first-order phase transition region while it exhibits a relatively obvious effect on the crossover region for smaller R, especially for $R = 3$ fm, which indicates that the small system size is indeed influential in the crossover region. Consequently, the location of the CEP also gets affected by the size of the fireball. And the CEPs for different chiral chemical potential and volume size are shown in Table I. It is worth noting that T of CEP decreases with reduction of system size R while rising with increasing chiral chemical potential μ_5. The μ of CEP is just the opposite. This agrees with the finding of Refs. [23,32,52,65,66].

TABLE I. The CEP for different volume size and chiral chemical potential.

	$\mu_5 = 0$ MeV		$\mu_5 = 100$ MeV		$\mu_5 = 300$ MeV	
CEP (MeV)	T	μ	T	μ	T	μ
$R = \infty$ fm	100	325	115	298	146	223
$R = 10$ fm	100	325	115	298	146	223
$R = 5$ fm	90	331	105	303	146	219
$R = 3$ fm	71	336	76	308	141	210

IV. SUMMARY AND CONCLUSIONS

We set out to investigate the finite volume effect on the chiral phase transition through two typical susceptibilities (χ_s and χ_T) with the two-flavor PNJL model at finite temperature T, chemical potential μ, and chiral chemical potential μ_5 within the mean-field approximation in this analysis. Our analysis contends that the phase diagram of finite system size above $R = 10$ fm almost totally overlaps with the counterpart of infinite system size at $\mu_5 = 0$ MeV, whereas the smaller R has a deviation in the crossover region where the chiral symmetry gets partially restored while the low temperature regions nearly stay still. On the other hand, the whole phase diagram of extremely small system size moves to the left at finite μ_5. In addition, T of the CEP reduces for smaller R. As a result, the tiny system size indeed has an impact on QCD susceptibilities at the crossover region, and smaller R exerts more evident influence, so that the volume of the QCD matter should be given more importance while studying the chiral phase transition and QCD phase structure. On the other hand, we find the chiral charge density n_5 decreases as system size gets smaller, suggesting an effect on the electric current induced by CME. We thereby find the finite volume effect contributes to various aspects of the heavy ion collision experiments.

ACKNOWLEDGMENTS

We are very grateful to Zhu-Fang Cui for conceiving the idea and providing constructive comments. This work is supported in part by the National Natural Science Foundation of China (under Grants No. 11805097, No. 11535005, No. 11690030, and No. 11905104), and the Jiangsu Provincial Natural Science Foundation of China under Grant No. BK20180323.

[1] M. Stephanov, K. Rajagopal, and E. Shuryak, Phys. Rev. Lett. **81**, 4816 (1998).
[2] S. P. Klevansky, Rev. Mod. Phys. **64**, 649 (1992).
[3] M. Buballa, Phys. Rept. **407**, 205 (2005).
[4] S. Roessner, C. Ratti, and W. Weise, Phys. Rev. D **75**, 034007 (2007).
[5] M. Stephanov, K. Rajagopal, and E. Shuryak, Phys. Rev. D **60**, 114028 (1999).
[6] Y. Hatta and M. Stephanov, Phys. Rev. Lett. **91**, 102003 (2003).
[7] M. A. Stephanov, Phys. Rev. D **73**, 094508 (2006).
[8] S. Ejiri, Phys. Rev. D **77**, 014508 (2008).
[9] B. Lungwitz and M. Bleicher, Phys. Rev. C **76**, 044904 (2007).
[10] A. Ayala, A. Bashir, J. Cobos-Martínez, S. Hernández-Ortiz, and A. Raya, Nucl. Phys. **B897**, 77 (2015).
[11] C. S. Fischer, J. Luecker, and C. A. Welzbacher, Phys. Rev. D **90**, 034022 (2014).
[12] G. Eichmann, C. S. Fischer, and C. A. Welzbacher, Phys. Rev. D **93**, 034013 (2016).
[13] V. V. Braguta, E.-M. llgenfritz, A. Y. Kotov, B. Petersson, and S. A. Skinderev, Phys. Rev. D **93**, 034509 (2016).
[14] H. Kohyama, D. Kimura, and T. Inagaki, Nucl. Phys. **B896**, 682 (2015).
[15] P. Kovács, Z. Szép, and G. Wolf, Phys. Rev. D **93**, 114014 (2016).
[16] C. Shi, Y.-L. Wang, Y. Jiang, Z.-F. Cui, and H.-S. Zong, J. High Energy Phys. 07 (2014) 014.
[17] L. Adamczyk *et al.*, Phys. Rev. Lett. **113**, 092301 (2014).
[18] R. Bruce. *et al.*, Phys. Rev. ST Accel. Beams **17**, 081004 (2014).
[19] R. A. Lacey, N. Ajitanand, J. Alexander, P. Chung, W. Holzmann, M. Issah, A. Taranenko, P. Danielewicz, and H. Stöcker, Phys. Rev. Lett. **98**, 092301 (2007).
[20] B. B. Abelev *et al.*, Int. J. Mod. Phys. A **29**, 1430044 (2014).
[21] E. Y. Loh, J. E. Gubernatis, R. T. Scalettar, S. R. White, D. J. Scalapino, and R. L. Sugar, Phys. Rev. B **41**, 9301 (1990).
[22] S. Chandrasekharan and U.-J. Wiese, Phys. Rev. Lett. **83**, 3116 (1999).
[23] A. Yamamoto, Phys. Rev. Lett. **107**, 031601 (2011).
[24] M. N. Chernodub and A. S. Nedelin, Phys. Rev. D **83**, 105008 (2011).
[25] M. Ruggieri, Phys. Rev. D **84**, 014011 (2011).
[26] R. Gatto and M. Ruggieri, Phys. Rev. D **85**, 054013 (2012).
[27] D. Ebert, T. Khunjua, K. Klimenko, and V. Zhukovsky, Phys. Rev. D **93**, 105022 (2016).
[28] V. V. Braguta and A. Y. Kotov, Phys. Rev. D **93**, 105025 (2016).
[29] K. Fukushima, M. Ruggieri, and R. Gatto, Phys. Rev. D **81**, 114031 (2010).
[30] V. V. Braguta, V. A. Goy, E. M. Ilgenfritz, A. Y. Kotov, A. V. Molochkov, M. Mller-Preussker, and B. Petersson, J. High Energy Phys. 06 (2015) 094.
[31] B. Wang, Y.-L. Wang, Z.-F. Cui, and H.-S. Zong, Phys. Rev. D **91**, 034017 (2015).
[32] S.-S. Xu, Z.-F. Cui, B. Wang, Y.-M. Shi, Y.-C. Yang, and H.-S. Zong, Phys. Rev. D **91**, 056003 (2015).
[33] G. Gräf, M. Bleicher, and Q. Li, Phys. Rev. C **85**, 044901 (2012).
[34] Y. Hirono and E. Shuryak, Phys. Rev. C **91**, 054915 (2015).
[35] P. Bożek and W. Broniowski, Phys. Lett. B **720**, 250 (2013).
[36] A. Bzdak, B. Schenke, P. Tribedy, and R. Venugopalan, Phys. Rev. C **87**, 064906 (2013).
[37] B. Klein, Phys. Rep. **707–708**, 1 (2017).
[38] Z. Fodor and S. Katz, J. High Energy Phys. 04 (2004) 050.
[39] G. Colangelo, S. Drr, A. Jttner, L. Lellouch, H. Leutwyler, V. Lubicz, S. Necco, C. T. Sachrajda, S. Simula, A. Vladikas, U. Wenger, and H. Wittig, Eur. Phys. J. C **71**, 1695 (2011).
[40] B. Orth, T. Lippert, and K. Schilling, Phys. Rev. D **72**, 014503 (2005).
[41] L. Giusti and S. Necco, J. High Energy Phys. 04 (2007) 090.
[42] J. Engels, S. Holtmann, T. Mendes, and T. Schulze, Phys. Lett. B **514**, 299 (2001).
[43] P. Hernández, K. Jansen, and L. Lellouch, Phys. Lett. B **469**, 198 (1999).
[44] J. B. Kogut and D. K. Sinclair, Phys. Rev. D **73**, 074512 (2006).
[45] J. Braun and B. Klein, Eur. Phys. J. C **63**, 443 (2009).
[46] M. H. Al-Hashimi, A. M. Shalaby, and U.-J. Wiese, Phys. Rev. D **95**, 065007 (2017).
[47] J. Casanova, C. Sabin, J. Leon, I. L. Egusquiza, R. Gerritsma, C. F. Roos, J. J. Garcia-Ripoll, and E. Solano, Phys. Rev. X **1**, 021018 (2011).
[48] L. Lamata, J. Casanova, and I. L. Egusquiza, and E. Solano, Phys. Scr. T **T147**, 014017 (2012).
[49] A. Mezzacapo, J. Casanova, L. Lamata, and E. Solano, New J. Phys. **15**, 033005 (2013).
[50] A. L. Gaunt, T. F. Schmidutz, I. Gotlibovych, R. P. Smith, and Z. Hadzibabic, Phys. Rev. Lett. **110**, 200406 (2013).
[51] A. Bhattacharyya, R. Ray, and S. Sur, Phys. Rev. D **91**, 051501 (2015).
[52] Z. Pan, Z.-F. Cui, C.-H. Chang, and H.-S. Zong, Int. J. Mod. Phys. A **32**, 1750067 (2017).
[53] C. S. Fischer and M. R. Pennington, Phys. Rev. D **73**, 034029 (2006).
[54] L. Fister and J. M. Pawlowski, Phys. Rev. D **92**, 076009 (2015).
[55] M. Ladrem and A. Ait-El-Djoudi, Eur. Phys. J. C **44**, 257 (2005).
[56] J. Luecker, C. S. Fischer, and R. Williams, Phys. Rev. D **81**, 094005 (2010).
[57] B.-Q. Ma, Q.-R. Zhang, D. Rischke, and W. Greiner, Phys. Lett. B **315**, 29 (1993).
[58] Y. Lu, Z.-F. Cui, Z. Pan, C.-H. Chang, and H.-S. Zong, Phys. Rev. D **93**, 074037 (2016).
[59] Z.-F. Cui, I. C. Cloët, Y. Lu, C. D. Roberts, S. M. Schmidt, S.-S. Xu, and H.-S. Zong, Phys. Rev. D **94**, 071503 (2016).
[60] A. Bhattacharyya, P. Deb, S. K. Ghosh, R. Ray, and S. Sur, Phys. Rev. D **87**, 054009 (2013).
[61] E. S. Fraga, L. F. Palhares, and P. Sorensen, Phys. Rev. C **84**, 011903 (2011).
[62] M. Cristoforetti, T. Hell, B. Klein, and W. Weise, Phys. Rev. D **81**, 114017 (2010).
[63] L. F. Palhares, E. S. Fraga, and T. Kodama, J. Phys. G **38**, 085101 (2011).
[64] C. Shi, W. Jia, A. Sun, L. Zhang, and H. Zong, Chin. Phys. C **42**, 023101 (2018).
[65] C. Shi, Y. Xia, W. Jia, and H. Zong, Sci. China Phys. Mech. Astron. **61**, 082021 (2018).

[66] B.-L. Li, Z.-F. Cui, B.-W. Zhou, S. An, L.-P. Zhang, and H.-S. Zong, Nucl. Phys. **B938**, 298 (2019).
[67] Q.-W. Wang, Y. Xia, and H.-S. Zong, Mod. Phys. Lett. A **33**, 1850232 (2018).
[68] Y.-P. Zhao, R.-R. Zhang, H. Zhang, and H.-S. Zong, Chin. Phys. C **43**, 063101 (2019).
[69] Z. Zhang, C. Shi, and H.-S. Zong, Phys. Rev. D **101**, 074036 (2020).
[70] K. Fukushima, Phys. Lett. B **591**, 277 (2004).
[71] Y. Sakai, T. Sasaki, H. Kouno, and M. Yahiro, Phys. Rev. D **82**, 076003 (2010).
[72] T. Hatsuda and T. Kunihiro, Phys. Rep. **247**, 221 (1994).
[73] J. M. Cornwall, Phys. Rev. D **26**, 1453 (1982).
[74] A. C. Aguilar, D. Binosi, and J. Papavassiliou, Phys. Rev. D **78**, 025010 (2008).
[75] A. Ayala, A. Bashir, D. Binosi, M. Cristoforetti, and J. Rodríguez-Quintero, Phys. Rev. D **86**, 074512 (2012).
[76] D. Binosi, L. Chang, J. Papavassiliou, and C. D. Roberts, Phys. Lett. B **742**, 183 (2015).
[77] S.-S. Xu, Z.-F. Cui, A. Sun, and H.-S. Zong, J. Phys. G **45**, 105001 (2018).
[78] Z.-F. Cui, S.-S. Xu, B.-L. Li, A. Sun, J.-B. Zhang, and H.-S. Zong, Eur. Phys. J. C **78**, 770 (2018).
[79] J. Gasser and H. Leutwyler, Phys. Lett. B **184**, 83 (1987).
[80] E. Shuryak and J. Verbaarschot, Nucl. Phys. **A560**, 306 (1993).
[81] J. Verbaarschot, Phys. Rev. Lett. **72**, 2531 (1994).
[82] J. Gasser and H. Leutwyler, Nucl. Phys. **B307**, 763 (1988).
[83] B. Borasoy and R. Lewis, Phys. Rev. D **71**, 014033 (2005).
[84] J. Braun, B. Klein, and H. J. Pirner, Phys. Rev. D **72**, 034017 (2005).
[85] J. Braun, B. Klein, and H. J. Pirner, Phys. Rev. D **71**, 014032 (2005).
[86] J. Braun, B. Klein, H.-J. Pirner, and A. H. Rezaeian, Phys. Rev. D **73**, 074010 (2006).
[87] G. Colangelo, S. Drr, and C. Haefeli, Nucl. Phys. **B721**, 136 (2005).
[88] A. A. Khan, T. Bakeyev, M. Gckeler, T. Hemmert, R. Horsley, A. Irving, B. Joó, D. Pleiter, P. Rakow, G. Schierholz, and H. Stben, Nucl. Phys. **B689**, 175 (2004).
[89] J. Verbaarschot and T. Wettig, Annu. Rev. Nucl. Part. Sci. **50**, 343 (2000).
[90] T. Kanazawa, T. Wettig, and N. Yamamoto, Phys. Rev. D **81**, 081701 (2010).
[91] Y.-P. Zhao, P.-L. Yin, Z.-H. Yu, and H.-S. Zong, Nucl. Phys. **B952**, 114919 (2020).
[92] Y.-L. Du, Z.-F. Cui, Y.-H. Xia, and H.-S. Zong, Phys. Rev. D **88**, 114019 (2013).
[93] S.-S. Xu, P.-L. Yin, and H.-S. Zong, Eur. Phys. J. C **79**, 399 (2019).